



OPEN ACCESS

EDITED BY

Fabio Grizzi,
Humanitas Research Hospital, Italy

REVIEWED BY

Baijun Dong,
Shanghai Jiao Tong University, China
Nil Tokgoz,
Gazi University, Türkiye

*CORRESPONDENCE

Tan-Hui Chen

✉ chenth0629@sina.com

Yan-Shun Lin

✉ 569091449@qq.com

†These authors share first authorship

RECEIVED 26 June 2023

ACCEPTED 02 October 2023

PUBLISHED 23 November 2023

CITATION

Zhao Y-Y, Xiong M-L, Liu Y-F, Duan L-J,
Chen J-L, Xing Z, Lin Y-S and Chen T-H
(2023) Magnetic resonance imaging
radiomics-based prediction of clinically
significant prostate cancer in equivocal PI-
RADS 3 lesions in the transitional zone.
Front. Oncol. 13:1247682.
doi: 10.3389/fonc.2023.1247682

COPYRIGHT

© 2023 Zhao, Xiong, Liu, Duan, Chen, Xing,
Lin and Chen. This is an open-access article
distributed under the terms of the [Creative
Commons Attribution License \(CC BY\)](#). The
use, distribution or reproduction in other
forums is permitted, provided the original
author(s) and the copyright owner(s) are
credited and that the original publication in
this journal is cited, in accordance with
accepted academic practice. No use,
distribution or reproduction is permitted
which does not comply with these terms.

Magnetic resonance imaging radiomics-based prediction of clinically significant prostate cancer in equivocal PI-RADS 3 lesions in the transitional zone

Ying-Ying Zhao^{1†}, Mei-Lian Xiong^{2†}, Yue-Feng Liu³,
Li-Juan Duan¹, Jia-Li Chen¹, Zhen Xing², Yan-Shun Lin^{1*}
and Tan-Hui Chen^{2*}

¹Department of Radiology, Fuqing City Hospital Affiliated to Fujian Medical University, Fuqing, China,

²Department of Radiology, The First Affiliated Hospital of Fujian Medical University, Fuzhou, China,

³Department of Ophthalmology Surgery, Taihe Hospital, Hubei University of Medicine, Shiyan, China

Purpose: This bi-institutional study aimed to establish a robust model for predicting clinically significant prostate cancer (csPCa) (pathological grade group ≥ 2) in PI-RADS 3 lesions in the transition zone by comparing the performance of combination models.

Materials and methods: This study included 243 consecutive men who underwent 3-Tesla magnetic resonance imaging (MRI) and ultrasound-guided transrectal biopsy from January 2020 and April 2022 which is divided into a training cohort of 170 patients and a separate testing cohort of 73 patients. T2WI and DWI images were manually segmented for PI-RADS 3 lesions for the mean ADC and radiomic analysis. Predictive clinical factors were identified using both univariate and multivariate logistic models. The least absolute shrinkage and selection operator (LASSO) regression models were deployed for feature selection and for constructing radiomic signatures. We developed nine models utilizing clinical factors, radiological features, and radiomics, leveraging logistic and XGboost methods. The performances of these models was subsequently compared using Receiver Operating Characteristic (ROC) analysis and the Delong test.

Results: Out of the 243 participants with a median age of 70 years, 30 were diagnosed with csPCa, leaving 213 without a csPCa diagnosis. Prostate-specific antigen density (PSAD) stood out as the only significant clinical factor (odds ratio [OR], 1.068; 95% confidence interval [CI], 1.029–1.115), discovered through the univariate and multivariate logistic models. Seven radiomic features correlated with csPCa prediction. Notably, the XGboost model outperformed eight other models (AUC of the training cohort: 0.949, and validation cohort: 0.913). However, it did not surpass the PSAD+MADC model ($P > 0.05$) in the training and testing cohorts (AUC, 0.949 vs. 0.888 and 0.913 vs. 0.854, respectively).

Conclusion: The machine learning XGboost model presented the best performance in predicting csPCa in PI-RADS 3 lesions within the transitional

zone. However, the addition of radiomic classifiers did not display any significant enhancement over the compound model of clinical and radiological findings. The most exemplary and generalized option for quantitative prostate evaluation was Mean ADC+PSAD.

KEYWORDS

magnetic resonance imaging, prostate cancer, PI-RADS, transitional zone, radiomics

1 Introduction

Prostate cancer is the most common cancer affecting men worldwide (1), with a lifetime risk as high as 37% (2). By 2040, global prostate cancer incidences are projected to rise to nearly 2.3 million new cases and 740 000 deaths (3). Multi-Magnetic resonance imaging (mpMRI) of the prostate, which helps improve the detection, localization, and staging of prostate cancer (PCa), has been established as the de facto standard for the imaging assessment of suspected PCa (4). A large-sample study demonstrated that utilizing MRI for initial screening before biopsy can minimize needless biopsies by approximately half for cases with a PI-RADS score of 3 or higher, and prevent the overdiagnosis of clinically insignificant lesions (5).

The Prostate Imaging Reporting and Data System (PI-RADS) has undergone continuous refinement and updates since its conception, allowing for more standardized assessments of prostate lesions. The most recent iteration, PI-RADSV2.1 revised in 2019, standardizes the terminology, interpretation, and contents of MRI reports (6). Lesions are classified into five categories (1 to 5), based on their anatomical location and MRI signal changes. Higher categories correlate with a higher probability of detecting clinically significant prostate cancer (csPCa). Lesions categorized as PI-RADS 1 and 2 bear an exceedingly low cancer detection rate (CDR) of less than 5% (7, 8) and necessitate only follow-up. In contrast, lesions classified as PI-RADS 4 and 5 have an extremely high CDR (40–80%) (7, 8) calling for further biopsy. However, PI-RADS 3 lesions present a moderate CDR, indicating an ambiguous risk of malignancy.

PI-RADS 3 lesions are frequently identified in patients undergoing MRI examinations, with reported incidences ranging from 22%–32% (9); However, most studies indicate a relatively low detection rate for csPCa, between 2%–22.9% (10, 11). Concurrently, the false negative rate for csPCa is notably high at 16.2% for cases with PI-RADS scores of 3 or higher (5). Current guidelines offer no explicit direction for subsequent treatment of PI-RADS 3 lesions, thereby presenting a dilemma for urologists in deciding between follow-up prostate-specific antigen (PSA) testing and imaging monitoring, or immediate biopsy. It is crucial to selectively submit patients likely to have csPCa to undergo prostate biopsy, maximizing the benefits from the procedure and potential aggressive treatment strategies.

Although the implementation of PI-RADSV2.1 has boosted the precision in identifying csPCa, PI-RADS 3 lesions remain elusive within the “gray zone” of mpMRI evaluations, especially for the transition zone (TZ). Benign prostatic hyperplasia, a common

condition in elderly men, creates a degree of organized chaos within the TZ, hampering accurate lesion categorization (12). Recent studies suggest exploiting radiomic features and mean apparent diffusion coefficient (ADC) values to quantitatively evaluate MRI enhances diagnostic accuracy for TZ lesions over mere qualitative PI-RADS assessment (13–15). Engel et al. reported that the risk stratification for prostatic TZ lesions could be improved through a quantitative diffusion-weighted imaging (DWI) analysis (4). Another study demonstrated an achievable specificity and sensitivity through downgrading PI-RADS lesions at or above 4 based on mean ADC values or machine learning algorithms (15). Ultimately, radiomics hold potential in algorithmically identifying csPCa in PI-RADS 3 lesions (13–16). A greater balance between biopsy-associated complications, overdiagnosis, and overlooking csPCa diagnosis might be achieved using radiomics prostate MRI. For patients with both PI-RADS 3 and a low risk of csPCa, immediate biopsy can possibly be deferred. However, previous studies of this nature typically involved smaller cohorts from a single institution and lacked distinction between PZ and TZ lesions (17).

Therefore, we hypothesized that the characteristics of detected TZ lesions can be improved through radiomics. This study aimed to assess different algorithm models for risk stratification among patients with PI-RADS 3 in the TZ, using a combination of individual clinical characteristics and radiological data.

2 Materials and methods

2.1 Demographic information and clinical data

This retrospective study included patients from two institutions (The First Affiliated Hospital of Fujian Medical University and Fuqing Hospital). The institutional ethics committee approved this study and waived the requirement for informed consent. Data were retrospectively collected from men who underwent MRI and biopsy examinations between January 2020 and April 2022 according to the following eligibility criteria: (a) men with PI-RADS 3 lesions (v2.1 standard), (b) PI-RADS 3 lesions confirmed by pathology and matched to the MR images in the same region, and (c) ultrasound-guided prostate biopsy or radical surgery performed within 1 month of the MRI examination. The exclusion criteria were: (a) biopsy or a history of treatment (antihormonal therapy, radiation therapy, focal

therapy, or prostatectomy) for prostate cancer prior to the MRI examination, (b) multiple primary cancers or a previous history of cancer, (c) incomplete sequences or severe artefacts on MRI images, and (d) any PI-RADS 4 or 5 lesions. **Figure 1** presents the flowchart of the inclusion and exclusion criteria of the study.

The following clinical and laboratory data were collected: age, the most recent serological value of total prostate-specific antigen (tPSA; ng/mL), free prostate-specific antigen (fPSA; ng/mL), fPSA/tPSA (f/t), prostate volume(V), PSA density (total PSA/prostatic volume ratio [PSAD]) during MRI examination and final histopathological analysis, and mean ADC value (mm²/s). The mean ADC value was calculated in volumes of interest (VOIs), encompassing the entire lesion without exceeding the lesion margins. **Table 1** presents the baseline epidemiologic and clinical characteristics, including tumor location, pathological findings, and clinical assessment.

A 12-core systematic biopsy was performed by urologists with three to five years of transrectal ultrasound-guided prostate biopsy experience. Based on biopsy results, the patients were divided into two cohorts: the csPCa and no csPCa (benign and Grade Group 1 [GG1]) groups. The primary endpoint of csPCa was defined as patients with ≥GG2 (Gleason 3 + 4) prostate cancer.

2.2 MRI examination

During the study period, prostate MRI was performed at Institution 1 using a 3.0T scanner (Spectra; Siemens Healthineers),

whereas it was performed using a 3.0T MRI system (Philips Ingenia, Amsterdam, the Netherlands) at Institution 2. Standard multichannel body coils and integrated spine phased-array coils were used according to the guidelines of the European Society of Urogenital Radiology (18). **Appendix Table 1** summarizes the details of the MRI protocols of each institution.

2.3 MRI lesion segmentation

To confirm that the lesions were classified as PI-RADS 3 as per the PI-RADS v2.1 guidelines, the MR images were interpreted by two radiologists (Y. Y. Z. and M. L. X.) with 6 and 10 years of experience in prostate MRI interpretation, respectively, who were blinded to the pathological data. In cases of disagreement, a final consensus was reached by re-reading.

Axial T2-weighted and diffusion-weighted images in DICOM format were downloaded from the picture archiving and communication system (PACS). The MRI index lesions were manually segmented by an investigator (Y. Y. Z.). Given the importance of heterogeneity analysis while avoiding partial volume effects, VOIs encompassing the entire lesion, including bleeding, necrosis, and cystic areas, the urethra, ejaculatory duct, and other normal anatomical structures were drawn on each slice with the lesion. Segmentation was performed under the supervision of another radiologist (T.H.C. with 20 years of experience in prostate MRI), using the dedicated software ITK-SNAP (version 3.8.0 for Win,

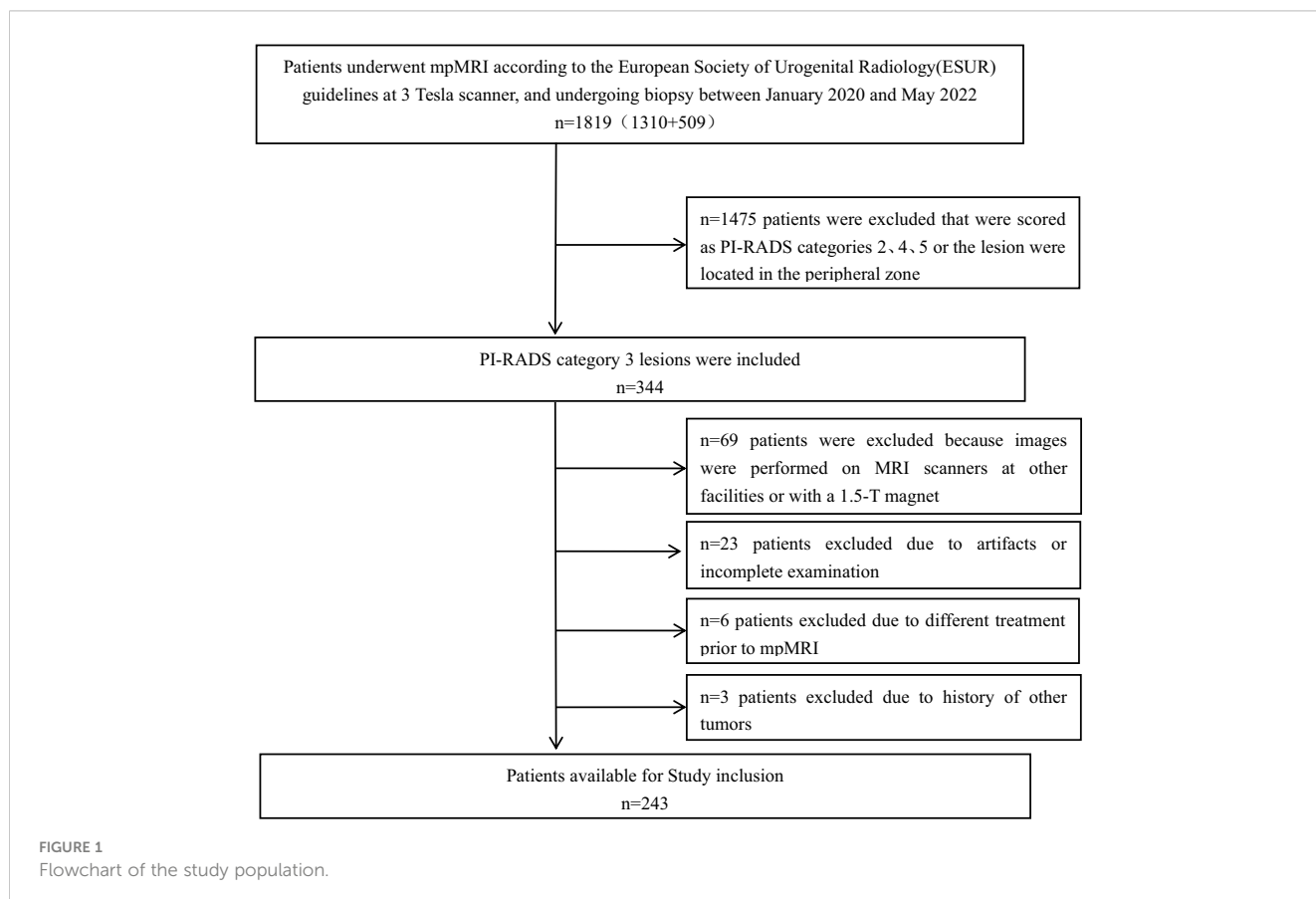


TABLE 1 The Characteristics of Demographic and Clinical Data of Patients with PIRADs 3 Lesions on MRI.

	level	Overall	No csPCa	csPCa	p
n		(n=243)	(n=213)	(n=30)	
GGG (%)	0	183 (75.3)	183 (85.9)	0 (0.0)	<0.001
	1	30 (12.3)	30 (14.1)	0 (0.0)	
	2	19 (7.8)	0 (0.0)	19 (63.3)	
	3	8 (3.3)	0 (0.0)	8 (26.7)	
	4	3 (1.2)	0 (0.0)	3 (10.0)	
age (median [IQR])		70	70	72	0.026
		[66.00, 75.00]	[65.00, 74.00]	[68.00, 76.00]	
MADC (median [IQR]×10 ⁻⁴)		8.22	8.39	6.98	<0.001
		[7.51, 8.83]	[7.68, 8.91]	[6.43, 7.75]	
MT2WI (median [IQR]×10 ²)		2.85	2.85	2.81	0.742
		[2.52, 3.38]	[2.54, 3.38]	[2.42, 3.53]	
RT2WI (median [IQR])		3.05	3.06	2.98	0.346
		[2.66, 3.40]	[2.66, 3.43]	[2.75, 3.18]	
V (median [IQR])		50	51.94	43.04	0.012
		[35.19, 66.60]	[35.70, 69.18]	[23.68, 52.56]	
PSAD (median [IQR]×10 ⁻²)		17.69	16.54	38.34	<0.001
		[10.10, 29.32]	[9.81, 25.38]	[19.19, 53.07]	
tPSA (median [IQR])		8.65	8.38	10.67	0.009
		[5.23, 13.55]	[5.07, 12.30]	[8.17, 19.18]	
fPSA (median [IQR])		1.45	1.42	1.94	0.029
		[0.95, 2.20]	[0.90, 2.14]	[1.35, 2.78]	
f/t (median [IQR])		0.17	0.17	0.13	0.044
		[0.12, 0.22]	[0.14, 0.22]	[0.10, 0.20]	

GGG, Gleason grade group; MADC, mean apparent diffusion coefficient; V, the volume of prostate; PSAD, prostate specific antigen density; tPSA, total prostate specific antigen; fPSA, free prostate specific antigen; f/t, fPSA/tPSA.

<http://www.itksnap.org/>). In addition, segmentation was also performed separately on axial T2-weighted and ADC images. The background obturator internus in the corresponding or adjacent layers was segmented for reference, excluding the muscle steatosis area while encompassing at least 50 voxels in at least three adjacent sections.

For the intraobserver and interobserver agreement evaluation in manual segmentation, we randomly selected 50 patients, and their ROIs were delineated 1 month later by the same radiologists (Y. Y. Z. and M. L. X.).

2.4 Image postprocessing and analysis

T2-weighted images were normalized by dividing the voxel intensities by the mean value of the background obturator internus tissue. Since ADC is a quantitative measurement, it was not normalized. Radiomic feature calculations were performed using the pyradiomics package of Python 3.7.1. (<https://github.com/>

Radiomics/pyradiomics) (18) according to the analytical steps depicted in Figure 2. Within each VOI, 14 volume and shape features, 198 first-order histogram features, 264 grey-level co-occurrence matrix (GLCM) features, 154 grey-level dependence matrix (GLDM) features, 176 grey-level run length matrix (GLRLM) features, 176 grey-level size zone matrix (GLSZM) features, and 55 neighboring grey tone difference matrix (NGTDM) features were calculated, resulting in 1037 features per VOI. These features were calculated on both the ADC maps and T2-weighted images; thus, a total of 2074 radiomics features were obtained for each lesion.

2.5 Radiomics feature selection and signature building

All patients were randomly stratified into the training and testing cohorts in a 7:3 ratio. The mean ADC was extracted from the

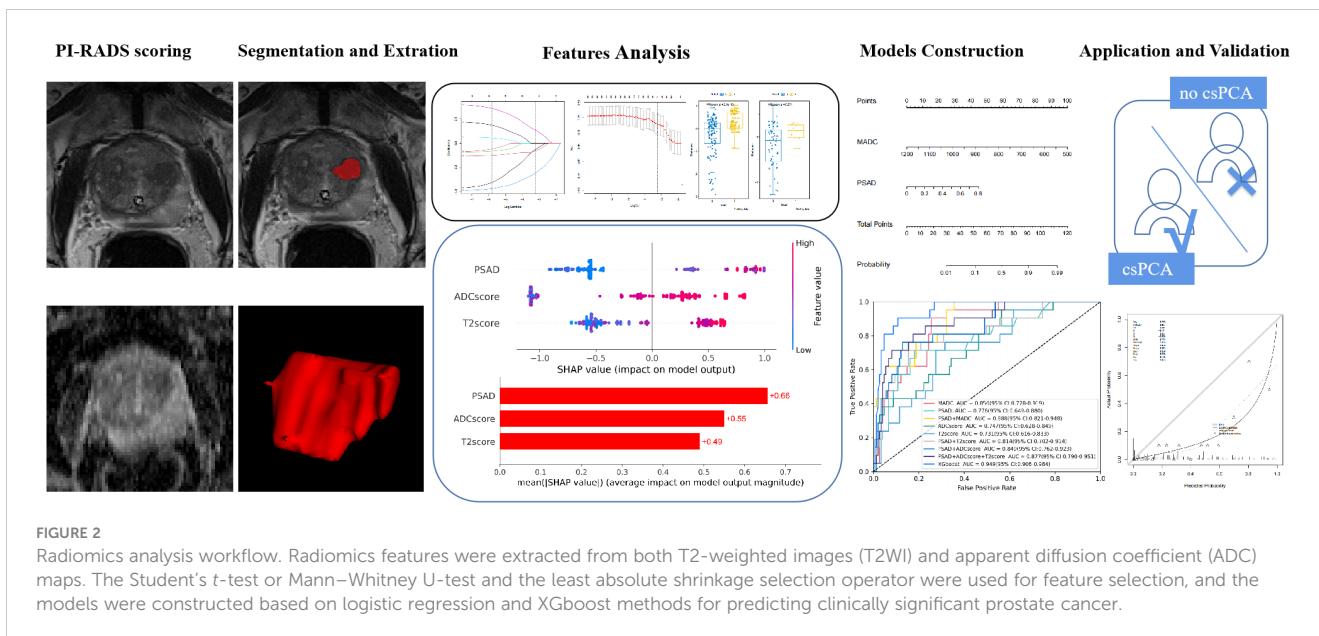


FIGURE 2 Radiomics analysis workflow. Radiomics features were extracted from both T2-weighted images (T2WI) and apparent diffusion coefficient (ADC) maps. The Student’s *t*-test or Mann–Whitney U-test and the least absolute shrinkage selection operator were used for feature selection, and the models were constructed based on logistic regression and XGboost methods for predicting clinically significant prostate cancer.

radiomic dataset for separate analyses. Missing data were analyzed using the Random Forest Multiple Interpolation method (R language mice package). The features with ICC < 0.75 were filtered out. Subsequently, upsampling was used to address sample imbalance in the training cohort, and the Student’s *t*-test or Mann–Whitney U-test was used for preliminary feature selection, which was determined using the Shapiro–Wilk and Levene’s tests. The least absolute shrinkage selection operator (LASSO)-logistic regression model was used to select the predictive features, and the radiomics signature (rad score) was calculated by adding the selected radiomics features, weighted by their respective coefficients. This procedure was performed separately on the T2-weighted and ADC images.

2.6 Creation and verification of model

Multivariate logistic regression analysis was used to identify independent predictive clinical factors. Prediction models were established based on clinical variables (clinical model), radiological features (radiological model), radiomic signatures (radiomics Model), and a combination of clinical variables, radiological features, and radiomics features (logistic regression and XGboost models) to generate a quantitative predictive tool for csPCa diagnosis. Calibration curves were used to evaluate the robustness of the model. Decision curve analysis (DCA) was used to evaluate the net benefit of the model for clinical decision-making at different threshold probabilities.

2.7 Statistical analysis

For demographic data, continuous variables were analyzed using Student’s *t*-test or Mann–Whitney U test, as determined by Shapiro–Wilk and Levene’s test. Continuous variables with normal distribution were presented as mean ± standard deviation.

Continuous variables with non-normal distribution were presented as median (inter-quartile range [IQR]). Categorical variables were analyzed using the chi-square test or Fisher’s exact test. Univariate and multivariate logistic regression analyses were used to identify the significant predictors of csPCa. LASSO logistic regression analysis was used for screening the predictive radiomics features. The eXtreme Gradient Boosting (XGboost) model was created with stratified 10-fold cross-validation, and a grid search was performed to identify the optimal hyperparameters for training using the GridSearchCV function in Scikit-learn (estimated by ten-fold cross-validation). The diagnostic performance of different models for the prediction of csPCa was assessed using receiver operating characteristic (ROC) curve analysis and by calculating the accuracy, sensitivity, specificity, and area under the ROC curve (AUC) with 95% CI. The Delong test was used to compare the performance of the different models, regardless of whether they differed significantly. All data analyses were performed using Python (version 4.0.1; <https://www.r-project.org>) and R (version 3.7.3; <https://www.python.org/downloads/>) software. All tests were two-sided, with statistical significance set at $P \leq 0.05$.

3 Results

3.1 Demographic information and clinical data

This study included 243 patients (median age, 70 years; IQR, 66–75 years). Prostate biopsy revealed that 213 (87.6%) patients did not have csPCa [183(75.3%) men had no cancer, and 30 (12.3%) had GG1], and 30 (12.3%) patients had csPCa. The detection rate for csPCa was equal to 13.7% (23/168 cases) vs 9.3% (7/75 cases) with PI-RADS 3 lesions diagnosed in the institution 1 vs the institution 2. The median PSA level was 8.65 ng/ml, with a mean prostate volume was 50.0 mL, and the median PSAD was 0.17 ng/mL². The patients were randomly allocated

to the training (N = 170) and testing (N = 73) cohorts. Table 1 presents the results of the comparison between the clinical factors of the csPCa and no csPCa groups.

3.2 Radiomics features selection and signature building

Initially, 2074 features were generated from the original T2-weighted and ADC imaging data, and 233 features related to csPCa diagnosis were selected. Highly correlated features were discarded (correlation between two variables > 0.6). Subsequently, the seven most predictive features were selected from the T2-weighted and ADC images using LASSO-logistic regression (Figure 3 and Table 2). The radiomic signature was then calculated by weighting their respective coefficients. The boxplot depicted in Figure 3 presents the differences between the two groups.

3.3 Development and validation of individualized logistic prediction models

Univariable logistic regression analysis of all potential factors identified age (odds ratio [OR], 1.075; 95% confidence interval [CI], 1.006–1.153), V (OR, 0.987; 95% CI, 0.974–0.998), PSAD (OR, 1.07; 95% CI, 1.034–1.113), and MADC (OR, 0.242; 95% CI, 0.126–0.422) as the independent parameters for csPCa prediction. When age, V, PSAD, and

MADC were included in the multivariate logistic regression analysis, only PSAD and MADC remained significantly correlated with tumor diagnosis (Table 3). Table 4 presents the eight models built for predicting csPCa using radiomics, a clinical variable, and the MADC values.

3.4 Development of the XGboost prediction model

Clinical factors (PSAD) and radiomic signatures were identified as the predictors most significantly associated with csPCa diagnosis. Therefore, these three features were employed as the input variables, whereas diagnostic efficiency was considered the output variance. The XGboost model hyperparameters were optimized using grid search and ten-fold cross-validation. The other parameters were set to default values. The detailed weights of the trained XGboost with the PSAD, T2 score, and ADC score for predicting csPCa are presented in Figure 4.

3.5 Performance comparisons of models

As shown in Tables 4, 5, and Figure 5, MADC was found to be the best-performing single-parameter model, with an AUC of 0.856 (95% CI, 0.782–0.923), and 0.788 (95% CI, 0.628–0.920) in the training and testing cohorts, respectively (Figure 4 and Table 4). The best combined models were PSAD + MADC (AUC, 0.888 [95% CI, 0.814–0.943], and

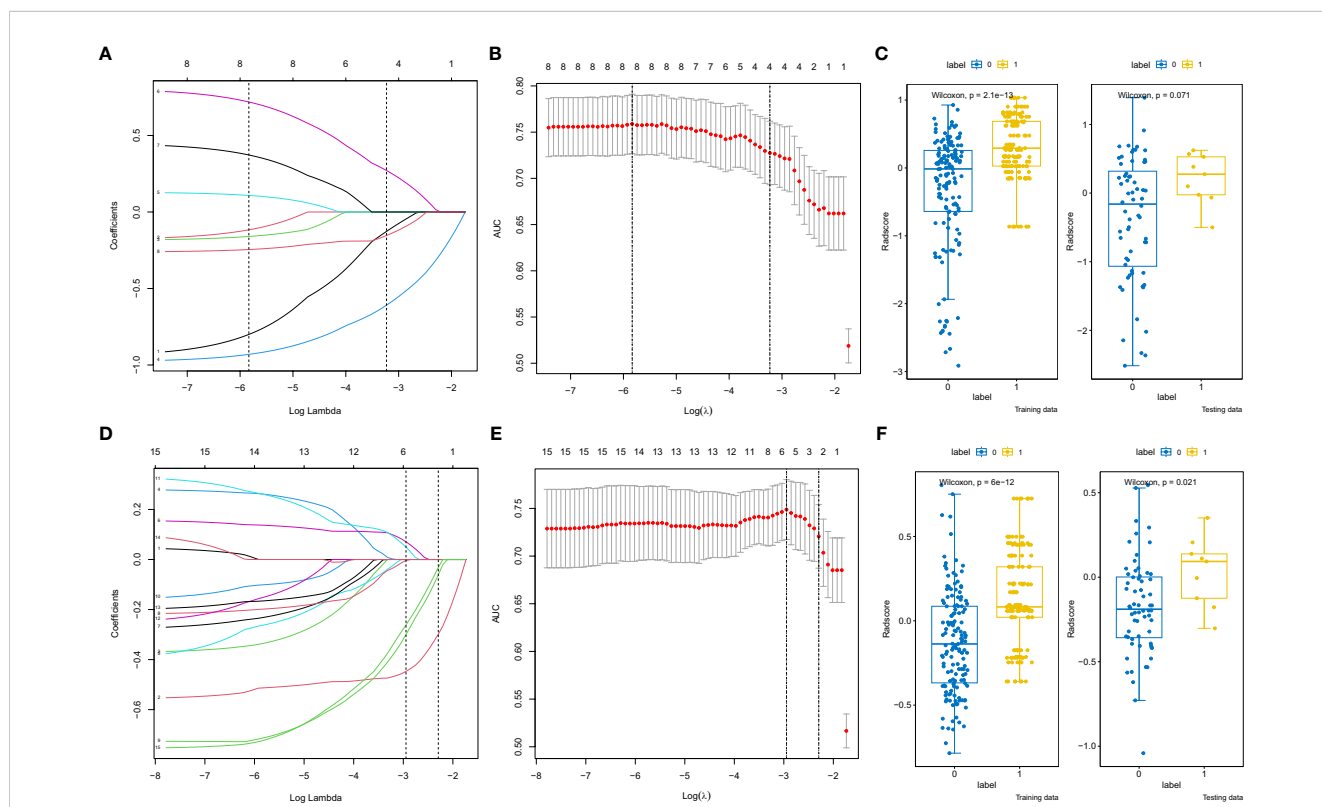


FIGURE 3 Radiomics features selection by the least absolute shrinkage selection operator. (A, D) Coefficient profiles of radiomics features of the apparent diffusion coefficient (ADC) and T2-weighted images (T2WI). (B, E) The adjustment penalty parameter λ is -3.229×10^{-4} and -2.294×10^{-4} for the ADC and T2WI, and seven features were selected according to 10-fold cross-validation. (C, F) The boxplot of radscores of the csPCa and No csPCa groups in the training and testing cohorts of the ADC and T2WI.

TABLE 2 The final 7 radiomics features selected from T2WI and ADC.

Features	Coef	OR
ADC.wavelet.HLH_glszm_SizeZoneNonUniformityNormalized	-0.60887	0.543965
ADC.wavelet.LLL_firorder_10Percentile	-0.15362	0.857601
ADC.exponential_firorder_Energy	-0.12684	0.880874
ADC.wavelet.HHL_glrmlm_LongRunHighGrayLevelEmphasis	0.270977	1.311245
T2WI.original_shape_Sphericity	-0.29877	0.741728
T2WI.wavelet.LHL_glcm_MCC	-0.06151	0.940344
T2WI.wavelet.LLL_gldm_LargeDependenceLowGrayLevelEmphasis	-0.03154	0.968952

0.854 [95% CI, 0.733–0.952] in the training and testing cohorts, respectively) and PSAD + ADC score + T2 score (0.877 [95% CI, 0.791–0.954], and 0.812 [95% CI, 0.684–0.920] in the training and testing cohorts, respectively) (Figure 5 and Table 4). However, they showed no evidence of improvement compared with the MADC model ($P = 0.162$ and $P = 0.687$ in the training cohorts, respectively, and $P = 0.303$ and $P = 0.818$ in the testing cohorts, respectively).

The XGboost model demonstrated the highest performance for predicting csPCa, with an AUC of 0.949 (95% CI, 0.904–0.983) and 0.913 (95% CI, 0.816–0.984) in the training and testing cohorts, respectively. Significant differences were observed between the AUCs of the XGboost model and the other five models (PSAD, ADC score, T2 score, PSAD + ADC score, and PSAD + ADC score + T2 score) (Figure 4 and Tables 4, 5). The AUCs of the training cohort were 0.949 vs. 0.778 vs. 0.747 vs. 0.731 vs. 0.849 vs. 0.877. The AUCs of the validation cohort were 0.913 vs. 0.620 vs. 0.688 vs. 0.740 vs. 0.757 vs. 0.812. However, it did not outperform the PSAD+MADC model (AUC, 0.949 vs. 0.888 and 0.913 vs. 0.854, respectively) ($P > 0.05$) in the training and testing cohorts, respectively.

4 Discussion

Precise definition of PI-RADS 3 lesions in the transition zone (TZ) presents a significant challenge due to the atypical imaging

features associated with these lesions. This is complicated by the reality that malignant epithelial cells often associated with csPCa are, in this classification, usually distributed sparsely and arranged around the acinar structures. Subsequently, csPCa imaging and benign conditions like hyperplasia, inflammation, and fibrosis can exhibit significant overlap (19). This can result in near imperceptible changes to MRI signal, leading to high rates of interpretation migration and fair inter-observer agreement (20). Furthermore, prostatic hyperplasia in elderly men, predominantly originating in the TZ, is intrinsically heterogeneous and comprises ill-defined tissues, often mistaken for csPCa due to their cellular and vascular nature (12). Currently, there is a shortage of effective means to refine lesion classification, leaving clinical management unclear.

Radiomic analysis provides a non-invasive tool using existing MRI images to obtain data about target organs and tissues. Its strength lies in eliminating subjective interpretation and observer reliance, concurrently analyzing hundreds of imaging features. This allows for a thorough characterization of tumor heterogeneity, reflecting tumor cellularity, proliferation, angiogenesis, hypoxia, and necrosis (21). Guiding classification, risk stratification, and clinical decision-making measures for suspicious lesions form key aspects of its performance duties (16, 22, 23). Consequently, radiomic analysis shows immense potential in distinguishing csPCAs from painless or benign cases (22, 23).

Several studies have probed into the function of radiomics in prostate imaging (24–26). Hou et al. evaluated radiomics machine

TABLE 3 Results of univariate and multivariate logistic regression analyses.

Facotrs	Uni_OR	Uni_95%CI	Uni_P	Mul_OR	Mul_95%CI	Mul_P
age	1.075	(1.006~1.153)	0.036	1.067	(0.968~1.178)	0.188
T	1.034	(0.99~1.076)	0.117	-	-	-
F	1.276	(0.969~1.654)	0.07	-	-	-
F/T	0.174	(0~1.228)	0.588	-	-	-
V	0.987	(0.974~0.998)	0.035	0.995	(0.981~1.008)	0.506
PSAD	1.07	(1.034~1.113)	<0.001	1.068	(1.029~1.115)	0.001
MT2WI	0.902	(0.525~1.373)	0.666	-	-	-
RT2WI	0.854	(0.356~1.96)	0.715	-	-	-
MADC	0.242	(0.126~0.422)	<0.001	0.231	(0.107~0.437)	<0.001

TABLE 4 The performance of different models in training and testing cohorts for predicting tumor diagnosis in csPca patients.

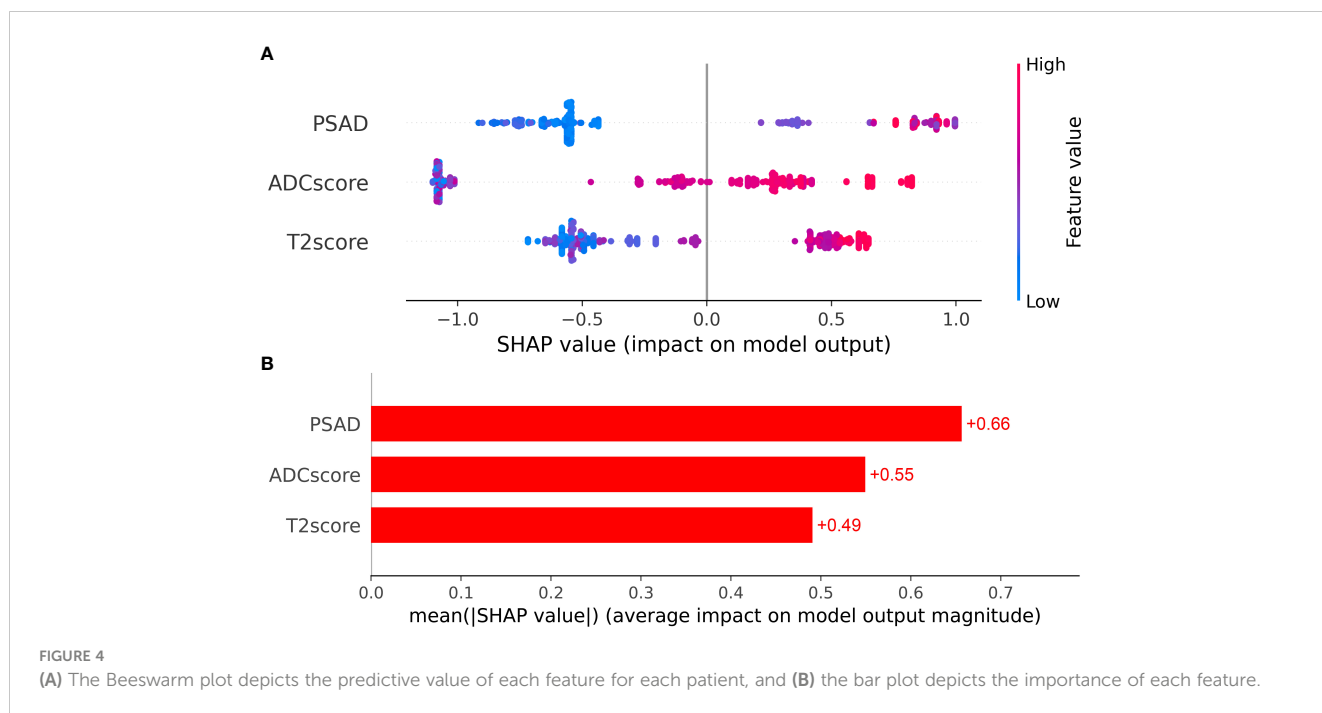
	Model	AUC (95% CI)	Accuracy	Sensitivity	Specificity
Training	MADC	0.856 (0.782-0.923)	0.765	0.905	0.745
	PSAD	0.778 (0.661-0.888)	0.806	0.714	0.819
	ADCscore	0.747 (0.640-0.850)	0.5	0.952	0.436
	T2score	0.731 (0.616-0.838)	0.694	0.762	0.685
	PSAD+MADC	0.888 (0.814-0.943)	0.688	1	0.644
	PSAD+T2score	0.814 (0.689-0.913)	0.829	0.714	0.846
	PSAD+ADCscore	0.849 (0.752-0.929)	0.859	0.762	0.872
	PSAD+ADCscore+T2score	0.877 (0.791-0.954)	0.824	0.81	0.826
	XGboost	0.949 (0.904-0.983)	0.894	0.905	0.893
Testing	MADC	0.788 (0.628-0.920)	0.699	0.778	0.688
	PSAD	0.620 (0.371-0.846)	0.795	0.556	0.828
	ADCscore	0.688 (0.540-0.818)	0.548	0.889	0.5
	T2score	0.740 (0.557-0.882)	0.767	0.556	0.797
	PSAD+MADC	0.854 (0.733-0.952)	0.63	0.889	0.594
	PSAD+T2score	0.809 (0.676-0.922)	0.781	0.556	0.812
	PSAD+ADCscore	0.757 (0.627-0.877)	0.74	0.333	0.797
	PSAD+ADCscore+T2score	0.812 (0.684-0.920)	0.822	0.667	0.844
	XGboost	0.913 (0.816-0.984)	0.904	0.889	0.906

MADC, mean ADC; PSAD, PSA density; XGboost, XGboost machine learning model.

learning (ML) models and reported an enhanced risk stratification, superior to subjective radiologist evaluation for identifying csPca in PI-RADS v2 category 3 lesions, with the AUC of radiomics ML models ranging from 0.87–0.89 (24). In a different study, Li et al. utilized a support vector machine (SVM) classification to stratify the Gleason Score (GS) of prostate cancer in the central gland using mpMRI. This approach showcased exceptional performance, with AUC values oscillating between 0.97 (CI 0.94–0.99) and 0.91 (CI 0.85–0.95) (25). Schelb et al. used a U-Net trained with T2-weighted and diffusion-weighted images, thereby achieving a performance on par with that of PI-RADS assessment (26). These studies collectively attest to the superior performance of radiomics in detecting prostate lesions.

Our study exhibits a classification capability that is, at the very least, comparable to those reported in the literature, thereby reiterating the utility of radiomics in prostate MRI. As reported in Table 4, the XGboost model showed the best performance, with AUC values of 0.949 and 0.913 in the training and testing cohorts, respectively. This indicates the XGboost model’s robust capacity to recognize csPca, indicating that machine learning’s potential as an efficient and noninvasive instrument for the prediction of csPca in PI-RADS 3 lesions. Commonly deployed to address classification issues, XGboost stands as the most accurate model for predicting 1-year survival among non-small cell lung cancer patients diagnosed with bone metastases (27). XGboost can also infer the tissue sources of 10 unique cancer types and outperforms traditional machine learning algorithms (28).

The predictive potential of clinical and radiological biomarkers for diagnosing prostate cancer associated with equivocal PI-RADS 3 lesions undergoing biopsy has been evaluated positively in previous studies (29, 30). For instance, Brancato et al. concluded that the most vital feature for the detection of cancer in PI-RADS 3 lesions was based on ADC maps (31). Our data also supported the use of quantitative ADC measurements for decision-making in PI-RADS 3 lesions, with AUC of 0.856 (0.782–0.923) and 0.788 (0.628–0.920) in the training and testing cohorts, respectively. Efficient at discerning the microenvironment of neoplastic tissues, ADC can identify alterations in compartmental volumes, such as stroma, epithelium, and lumen space, and cellularity (32). It currently serves as best parameter for prostate MRI assessment (4, 33). Moreover, ADC has been consistently proven to be inversely correlated with factors like tumor grade, tumor aggressiveness, and pathological stage (34–36). We compared the performance of the mean ADC with biparametric radiomics to assess whether it had an added value over that of machine learning. The Delong test results revealed superior performance from XGboost models as opposed to the mean ADC model in the training cohorts. However, this superiority was not replicated in the testing cohorts. Moreover, it did not outperform the PSAD+MADC model (AUC, 0.949 vs. 0.888 and 0.913 vs. 0.854, respectively) ($P > 0.05$) in both the training and testing cohorts. Thus, within the context of our study, ADC values remained the most decisive parameter, aligning with previous studies’ findings (33, 36). Bonekamp et al. (36) compared the performance of biparametric contrast-free radiomics with that of



machine learning for detecting csPCa, also concluded that the performance of radiomic machine learning did not exceed that of the mean ADC. This finding is coherent with the results observed in our study.

However, several differences from the present study should be noted. Prior studies did not conduct separate analyses for peripheral zone (PZ) and TZ lesions. Given that the lesion characteristics significantly differ between PZ and TZ, and the primary sequences vary, it is recommended to perform targeted analysis based on lesions in different zones rather than combining them. Second,

some studies exploring the intelligent diagnosis of PI-RADS 3 lesions were confined to basic radiomic features (33, 35, 36) and overlooked the additional diagnostic value of clinical indicators. Compared with these similar studies, the present study evaluated clinical features associated with csPCa, encompassing age, tPSA, fPSA, fPSA/tPSA, prostate volume, and PSA density. However, only one of these, specifically PSAD, proved useful for building predictive models.

MRI application as an adjuvant examination rather than a clinical triage tool can pose challenges, considering negative

TABLE 5 The performance comparisons of different models in training and testing cohorts.

Model	MADC	PSAD	PSAD + MADC	ADCscore	T2score	PSAD + T2score	PSAD + ADCscore	PSAD + ADCscore + T2score	XGboost
MADC	/	0.219	0.162	0.099	0.046	0.505	0.909	0.687	0.023
PSAD	0.322	/	0.014	0.674	0.467	0.247	0.019	0.005	0.000
PSAD + MADC	0.303	0.06	/	0.031	0.007	0.132	0.357	0.805	0.075
ADCscore	0.367	0.684	0.078	/	0.857	0.38	0.047	0.018	0.000
T2score	0.653	0.519	0.295	0.534	/	0.049	0.061	0.002	0.000
PSAD + T2score	0.846	0.043	0.513	0.19	0.493	/	0.377	0.022	0.001
PSAD + ADCscore	0.771	0.183	0.146	0.337	0.88	0.304	/	0.18	0.004
PSAD + ADCscore + T2score	0.818	0.158	0.611	0.017	0.34	0.953	0.307	/	0.003
XGboost	0.133	0.038	0.368	0.000	0.008	0.098	0.015	0.018	/

Based on Delong.test, the upper right of the diagonal (yellow) was the P value of model comparisons in the training set, and the down left of the diagonal (blue) was the P value of model comparisons in the testing set.

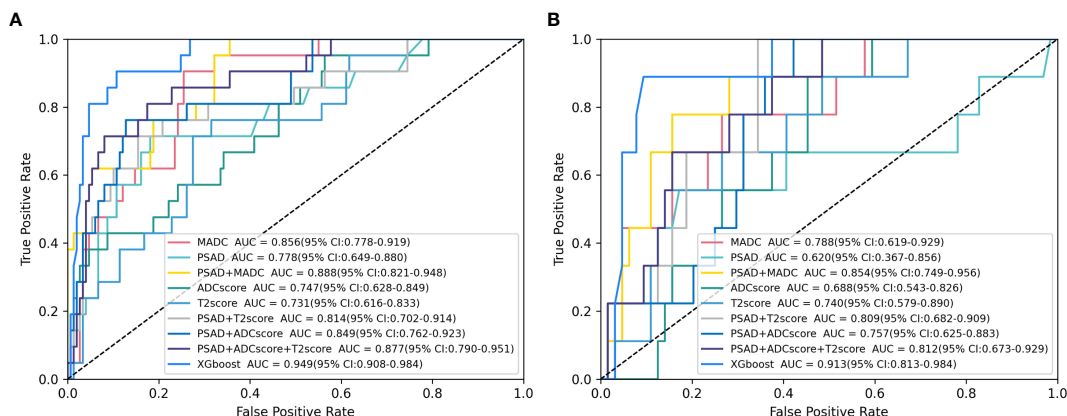


FIGURE 5

Receiver operating characteristic (ROC) analysis of the parameter models in clinically significant prostate cancer (csPCa) of PI-RADS 3 Lesions prediction. (A, B) ROC curves for selected logistic models and XGboost models tested for csPCa prediction in the (A) training cohort and (B) testing cohort. Plus signs indicate parameter combinations in the multivariable models, and data in brackets are 95% confidence intervals. See Table 4 for corresponding area under the ROC curve (AUC) values and additional models.

findings do not necessarily discourage further progression to a biopsy, potentially leading to overtreatment (37). Integrating MRI findings with PSAD may mitigate these concerns. PSAD also constitutes an essential component of the best-performing XGboost model in this study, and has been extensively investigated in several studies (38–40). A large multi-institutional collaborative study showed that among the men with a solitary PI-RADS 3 lesion on MRI, nearly 87% of those with a low PSAD had no or only GG1 prostate cancer. In contrast, as PSAD increases, the rate of csPCa detection increases to more than one-third of men biopsied (37). Several studies have identified an independent association of PSAD with csPCa, even in patients with serum PSA levels slightly exceeding or within the normal range—a common occurrence across various clinical scenarios, such as early diagnosis, repeat biopsy, and active surveillance (38). Roscigno et al. (39) reported that higher PSAD was associated with an elevated risk of reclassification, with 0.20 as the threshold in definitive or follow-up biopsy. Washino et al. (40) increased the negative predictive value (NPV) of PI-RADS from 0.84 to 0.96 by using PSAD with a cut-off value of 0.15 ng/mL/cc. Ullrich et al. (41) concluded that if the PSAD cut-off was 0.15 ng/mL², 53% of patients with a PI-RADS v2 score of 3 would have avoided biopsy.

In our study, the predictive performance of radiomics machine learning models did not surpass that of the comprehensive model combining clinical variables and radiological features (MADC + PSAD). This may change with the development of next-generation machine learning techniques for larger-scale cohorts in multicentric setups, as machine learning methods rely on large amounts of training and testing data. These tools typically do not require segmentation or handcrafted radiomic features. In the current study, more traditional machine learning methods were used due to the relatively small sample size and number of csPCa cases.

Our study had several limitations. The retrospective design of this study, combined with the lack of results from radical prostatectomy specimens as a reference standard, means that

selection bias and biopsy bias are potential issues. In addition, the PI-RADS 3 dataset is notably small and imbalanced. A more sizable, balanced study group would better facilitate radiomic analyses and aid in formulating robust predictive models. Lastly, identifying PI-RADS 3 lesions can prove challenging, making some lesions ambiguous.

5 Conclusions

Radiomics-based algorithms, notably the XGboost models, demonstrated substantial proficiency in predicting csPCa in PI-RADS 3 lesions in TZ. This could potentially elevate the rate of prostate-positive biopsy for PI-RADS 3 while decreasing the incidence of unnecessary biopsies. Predictions yielded by the XGboost classifier could serve as a crucial reference for clinical decision-making. However, in the current cohort, no additional benefits of the radiomic classifiers were observed over the combined model of clinical and radiological findings, suggesting the mean ADC+PSAD as the most generalized and optimal choice for quantitative prostate assessment.

Data availability statement

The original contributions presented in the study are included in the article/supplementary material. Further inquiries can be directed to the corresponding authors.

Ethics statement

The studies involving humans were approved by ethics committee of Fuqing City Hospital Affiliated to Fujian Medical University. The studies were conducted in accordance with the local

legislation and institutional requirements. The participants provided their written informed consent to participate in this study. Written informed consent was obtained from the individual(s) for the publication of any potentially identifiable images or data included in this article.

Author contributions

T-HC and Y-SL established the central thrust of our study. Y-YZ and M-LX drafted the manuscript, which was revised by ZX, and L-JD. Y-FL and J-LC analyzed the research data. All authors contributed to the article and approved the submitted version.

Funding

Our study was funded by the Fuzhou Health System Science and Technology Plan Project (2022-S-wq-17) and the Startup Fund for scientific research of Fujian Medical University (No. 2019QH1097).

References

1. Siegel RL, Miller KD, Fuchs HE, Jemal A. Cancer statistics, 2022. *CA Cancer J Clin* (2022) 72:7–33. doi: 10.3322/caac.21708
2. Siegel RL, Miller KD, Fuchs HE, Jemal A. Cancer statistics, 2021. *CA Cancer J Clin* (2021) 71:7–33. doi: 10.3322/caac.21654
3. Ferlay J, Ervik M, Lam F, Colombet M, Mery L, Piñeros M, et al. *Global cancer observatory: cancer today*. International Agency for Research on Cancer: Lyon, France (2020). Available at: <https://gco.iarc.fr/today>.
4. Engel H, Oerther B, Reiser M, Kellner E, Sigle A, Gratzke C, et al. Quantitative analysis of diffusion weighted imaging may improve risk stratification of prostatic transition zone lesions. *In Vivo* (2022) 36:2323–31. doi: 10.21873/invivo.12963
5. Pepe P, Garufi A, Priolo GD, Galia A, Frassetto F, Pennisi M. Is it time to perform only magnetic resonance imaging targeted cores? Our experience with 1,032 men who underwent prostate biopsy. *J Urol* (2018) 200(4):774–8. doi: 10.1016/j.juro.2018.04.061
6. Turkbey B, Rosenkrantz AB, Haider MA, Padhani AR, Villeirs G, Macura KJ, et al. Prostate imaging reporting and data system version 2.1: 2019 update of prostate imaging reporting and data system version 2. *Eur Urol* (2019) 76:340–51. doi: 10.1016/j.eururo.2019.02.033
7. Wang ZB, Wei CG, Zhang YY, Pan P, Dai GC, Tu J, et al. The Role of PSA Density among PI-RADS v2.1 Categories to Avoid an Unnecessary Transition Zone Biopsy in Patients with PSA 4–20 ng/mL. *BioMed Res Int* (2021) 2021:3995789. doi: 10.1155/2021/3995789
8. Oerther B, Engel H, Bamberg F, Sigle A, Gratzke C, Benndorf M. Cancer detection rates of the PI-RADSV2.1 assessment categories: systematic review and meta-analysis on lesion level and patient level. *Prostate Cancer Prostatic Dis* (2022) 25:256–63. doi: 10.1038/s41391-021-00417-1
9. Moldovan PC, Van den Broeck T, Sylvester R, Marconi L, Bellmunt J, van den Bergh RCN, et al. What is the negative predictive value of multiparametric magnetic resonance imaging in excluding prostate cancer at biopsy? A systematic review and meta-analysis from the European association of urology prostate cancer guidelines panel. *Eur Urol* (2017) 72:250–66. doi: 10.1016/j.eururo.2017.02.026
10. Thaiss WM, Moser S, Hepp T, Kruck S, Rausch S, Scharpf M, et al. Head-to-head comparison of biparametric versus multiparametric MRI of the prostate before robot-assisted transperineal fusion prostate biopsy. *World J Urol* (2022) 40:2431–8. doi: 10.1007/s00345-022-04120-1
11. Stabile A, Dell'Oglio P, De Cobelli F, Esposito A, Gandaglia G, Fossati N, et al. Association between prostate imaging reporting and data system (PI-RADS) score for the index lesion and multifocal, clinically significant prostate cancer. *Eur Urol Oncol* (2018) 1:29–36. doi: 10.1016/j.euo.2018.01.002
12. Weinreb JC. Organized chaos: does PI-RADS version 2 work in the transition zone? *Radiology* (2018) 288:492–4. doi: 10.1148/radiol.2018180123
13. Woźnicki P, Westhoff N, Huber T, Riffel P, Froelich MF, Gresser E, et al. Multiparametric MRI for prostate cancer characterization: combined use of radiomics

Acknowledgments

We are extremely grateful for the support and help from our department at the First Affiliated Hospital of Fujian Medical University.

Conflict of interest

The authors declare that the research was conducted in the absence of any commercial or financial relationships that could be construed as a potential conflict of interest.

Publisher's note

All claims expressed in this article are solely those of the authors and do not necessarily represent those of their affiliated organizations, or those of the publisher, the editors and the reviewers. Any product that may be evaluated in this article, or claim that may be made by its manufacturer, is not guaranteed or endorsed by the publisher.

model with PI-RADS and clinical parameters. *Cancers (Basel)* (2020) 12:1767. doi: 10.3390/cancers12071767

14. Wu M, Krishna S, Thornhill RE, Flood TA, McInnes MDF, Schieda N. Transition zone prostate cancer: Logistic regression and machine-learning models of quantitative ADC, shape and texture features are highly accurate for diagnosis. *J Magn Reson Imaging* (2019) 50:940–50. doi: 10.1002/jmri.26674

15. Zhang KS, Schelb P, Kohl S, Radtke JP, Wiesenfarth M, Schimmöller L, et al. Improvement of PI-RADS-dependent prostate cancer classification by quantitative image assessment using radiomics or mean ADC. *Magn Reson Imaging* (2021) 82:9–17. doi: 10.1016/j.mri.2021.06.013

16. Hectors SJ, Chen C, Chen J, Wang J, Gordon S, Yu M, et al. Magnetic resonance imaging radiomics-based machine learning prediction of clinically significant prostate cancer in equivocal PI-RADS 3 lesions. *J Magn Reson Imaging* (2021) 54:1466–73. doi: 10.1002/jmri.27692

17. Kan Y, Zhang Q, Hao J, Wang W, Zhuang J, Gao J, et al. Clinico-radiological characteristic-based machine learning in reducing unnecessary prostate biopsies of PI-RADS 3 lesions with dual validation. *Eur Radiol* (2020) 30:6274–84. doi: 10.1007/s00330-020-06958-8

18. Barentsz JO, Richenberg J, Clements R, Choyke P, Verma S, Villeirs G, et al. ESUR prostate MR guidelines 2012. *Eur Radiol* (2012) 22:746–57. doi: 10.1007/s00330-011-2377-y

19. Jin P, Yang L, Qiao X, Hu C, Hu C, Wang X, et al. Utility of clinical-radiomic model to identify clinically significant prostate cancer in biparametric MRI PI-RADS V2.1 category 3 lesions. *Front Oncol* (2022) 12:840786. doi: 10.3389/fonc.2022.840786

20. Westphalen AC, McCulloch CE, Anaokar JM, Arora S, Barashi NS, Barentsz JO, et al. Variability of the positive predictive value of PI-RADS for prostate MRI across 26 centers: experience of the society of abdominal radiology prostate cancer disease-focused panel. *Radiology* (2020) 296:76–84. doi: 10.1148/radiol.2020190646

21. Ganeshan B, Goh V, Mandeville HC, Ng QS, Hoskin PJ, Miles KA. Non-small cell lung cancer: histopathologic correlates for texture parameters at CT. *Radiology* (2013) 266:326–36. doi: 10.1148/radiol.12112428

22. Liddell H, Jyoti R, Haxhimolla HZ. Mp-MRI prostate characterised PIRADS 3 lesions are associated with a low risk of clinically significant prostate cancer - A retrospective review of 92 biopsied PIRADS 3 lesions. *Curr Urol* (2015) 8:96–100. doi: 10.1159/000365697

23. Xiong H, He X, Guo D. Value of MRI texture analysis for predicting high-grade prostate cancer. *Clin Imaging* (2021) 72:168–74. doi: 10.1016/j.clinimag.2020.10.028

24. Hou Y, Bao ML, Wu CJ, Zhang J, Zhang YD, Shi HB. A radiomics machine learning-based redefining score robustly identifies clinically significant prostate cancer in equivocal PI-RADS score 3 lesions. *Abdom Radiol (NY)* (2020) 45:4223–34. doi: 10.1007/s00261-020-02678-1

25. Li J, Weng Z, Xu H, Zhang Z, Miao H, Chen W, et al. Support Vector Machines (SVM) classification of prostate cancer Gleason score in central gland using

multiparametric magnetic resonance images: A cross-validated study. *Eur J Radiol* (2018) 98:61–7. doi: 10.1016/j.ejrad.2017.11.001

26. Schelb P, Kohl S, Radtke JP, Wiesenfarth M, Kickingereder P, Bickelhaupt S, et al. Classification of Cancer at Prostate MRI: Deep Learning versus Clinical PI-RADS Assessment. *Radiology* (2019) 293:607–17. doi: 10.1148/radiol.2019190938
27. Huang Z, Hu C, Chi C, Jiang Z, Tong Y, Zhao C. An artificial intelligence model for predicting 1-year survival of bone metastases in non-small-cell lung cancer patients based on XGBoost algorithm. *BioMed Res Int* (2020) 2020:3462363. doi: 10.1155/2020/3462363
28. Zhang Y, Feng T, Wang S, Dong R, Yang J, Su J, et al. A novel XGBoost method to identify cancer tissue-of-origin based on copy number variations. *Front Genet* (2020) 11:585029. doi: 10.3389/fgene.2020.585029
29. Sheridan AD, Nath SK, Syed JS, Aneja S, Sprenkle PC, Weinreb JC, et al. Risk of clinically significant prostate cancer associated with prostate imaging reporting and data system category 3 (Equivocal) lesions identified on multiparametric prostate MRI. *AJR Am J Roentgenol* (2018) 210:347–57. doi: 10.2214/AJR.17.18516
30. Lim CS, Abreu-Gomez J, Leblond MA, Carrion I, Vesprini D, Schieda N, et al. When to biopsy Prostate Imaging and Data Reporting System version 2 (PI-RADSV2) assessment category 3 lesions? Use of clinical and imaging variables to predict cancer diagnosis at targeted biopsy. *Can Urol Assoc J* (2021) 15:115–21. doi: 10.5489/auaj.6781
31. Brancato V, Aiello M, Basso L, Monti S, Palumbo L, Di Costanzo G, et al. Evaluation of a multiparametric MRI radiomic-based approach for stratification of equivocal PI-RADS 3 and upgraded PI-RADS 4 prostatic lesions. *Sci Rep* (2021) 11:643. doi: 10.1038/s41598-020-80749-5
32. Schieda N, Lim CS, Zabihollahy F, Abreu-Gomez J, Krishna S, Woo S, et al. Quantitative prostate MRI. *J Magn Reson Imaging* (2021) 53:1632–45. doi: 10.1002/jmri.27191
33. Tavakoli AA, Hielscher T, Badura P, Görtz M, Kuder TA, Gnirs R, et al. Contribution of dynamic contrast-enhanced and diffusion MRI to PI-RADS for detecting clinically significant prostate cancer. *Radiology* (2023) 306:186–99. doi: 10.1148/radiol.212692
34. Surov A, Meyer HJ, Wienke A. Correlations between apparent diffusion coefficient and gleason score in prostate cancer: A systematic review. *Eur Urol Oncol* (2020) 3:489–97. doi: 10.1016/j.euo.2018.12.006
35. Lim C, Flood TA, Hakim SW, Shabana WM, Quon JS, El-Khodary M, et al. Evaluation of apparent diffusion coefficient and MR volumetry as independent associative factors for extra-prostatic extension (EPE) in prostatic carcinoma. *J Magn Reson Imaging* (2016) 43:726–36. doi: 10.1002/jmri.25033
36. Bonekamp D, Kohl S, Wiesenfarth M, chelb P, Radtke JP, Götz M, et al. Radiomic machine learning for characterization of prostate lesions with MRI: comparison to ADC values. *Radiology* (2018) 289:128–37. doi: 10.1148/radiol.2018173064
37. Drevik J, Dalimov Z, Uzzo R, Danella J, Guzzo T, Belkoff L, et al. Utility of PSA density in patients with PI-RADS 3 lesions across a large multi-institutional collaborative. *Urol Oncol* (2022) 40:490.e1–6. doi: 10.1016/j.urolonc.2022.08.003
38. Galosi AB, Palagonia E, Scarcella S, Cimadamore A, Lacetera V, Delle Fave RF, et al. Detection limits of significant prostate cancer using multiparametric MR and digital rectal examination in men with low serum PSA: Up-date of the Italian Society of Integrated Diagnostic in Urology. *Arch Ital Urol Androl* (2021) 93:92–100. doi: 10.4081/aiua.2021.1.92
39. Roscigno M, Stabile A, Lughezzani G, Pepe P, Galosi AB, Naselli A, et al. The use of multiparametric magnetic resonance imaging for follow-up of patients included in active surveillance protocol. Can PSA density discriminate patients at different risk of reclassification? *Clin Genitourin Cancer* (2020) 18:e698–704. doi: 10.1016/j.clgc.2020.04.006
40. Washino S, Okochi T, Saito K, Konishi T, Hirai M, Kobayashi Y, et al. Combination of prostate imaging reporting and data system (PI-RADS) score and prostate-specific antigen (PSA) density predicts biopsy outcome in prostate biopsy naïve patients. *BJU Int* (2017) 119:225–33. doi: 10.1111/bju.13465
41. Ullrich T, Quentin M, Arsov C, Schmaltz AK, Tschischka A, Laqua N, et al. Risk stratification of equivocal lesions on multiparametric magnetic resonance imaging of the prostate. *J Urol* (2018) 199:691–8. doi: 10.1016/j.juro.2017.09.074

Appendix

APPENDIX 1 Acquisition Parameters of the Multiparametric MRI Protocol for both institution.

Parameter	T2WI		DWI	
	Institution 1	Institution 2	Institution 1	Institution 2
Echo time (msec)	72	93	72	93
Repetition time (msec)	4000	5960	4000	6900
Flip angle (°)	90	150	–	–
Matrix	128×128	256×256	128×128	256×256
Field of view (mm ²)	360×360	160×160	360×360	190×260
Number of slices	36	40	32	40
Slice thickness (mm)	4	3	4	3
spacing between slices	0.5	0	1	0
b-values (s/mm ²)	–	–	100/800/2000	50/800/1500